Influence of the shape of the strut cross section on the hydrodynamics and heat transfer of laminar steady-state flow in Kelvin cell based POCS

Project Report

by

Anish Anand Pophale

Department of Chemical Engineering
Indian Institute of Technology Madras

Supervisors

M.Sc. Katharina Knapp

Institute of Thermal Process Engineering
Karlsruhe Institute of Technology

Prof. Dr.-Ing. Thomas Wetzel

Institute of Thermal Process Engineering
Karlsruhe Institute of Technology

Contents

List of Symbols

λ	Thermal Conductivity
μ	Viscosity
ν	Kinematic Viscosity
ψ	Porosity
ρ	Density
d_c	Cell dimension
d_s	Strut diameter
h	Heat Transfer Coefficient
Hg	Hagen Number
L	Strut Length
L_{char}	Characteristic Length Scale
$MAPE$	Mean Average Percentage Error
Nu	Nusselt Number
P	Pressure
$POCS$	Periodic Open Cellular Structures
Re	Reynolds Number
s_L	Dimensionless longitudinal pitch
s_T	Dimensionless transverse pitch
T	Temperature
v	Average Velocity
v_o	Superficial Velocity
Pr	Prandtl Number

1 Introduction

Periodic Open Cellular Structures (POCS) are a novel class of porous materials consisting of continuous, interconnected solid and fluid phases with highly ordered and repeating geometries. Such porous materials are used in a wide range of applications such as for lightweight structures, biomedical implants, catalyst supports and heat exchangers because their high specific surface area, low pressure drop and good heat transfer and mechanical properties.

POCS can be manufactured via additive manufacturing techniques and one of the main advantages of these materials is the design freedom. A unit cell is the basic repeating structure which makes up POCS. Each unit cell consists of struts which are connected to each other via nodes, and different arrangements of these struts and nodes lead of various types of unit cells such as the Cubic, Staggered Cubic, Inclined and Doubly Inclined Cubic, Diamond, Kelvin, etc. cells as shown in Fig 1. Depending on the choice of the unit cell as well as other parameters such as the strut diameter, strut shape, unit cell dimension, porosity, etc. the design of the POCS can be tailored for specific applications.

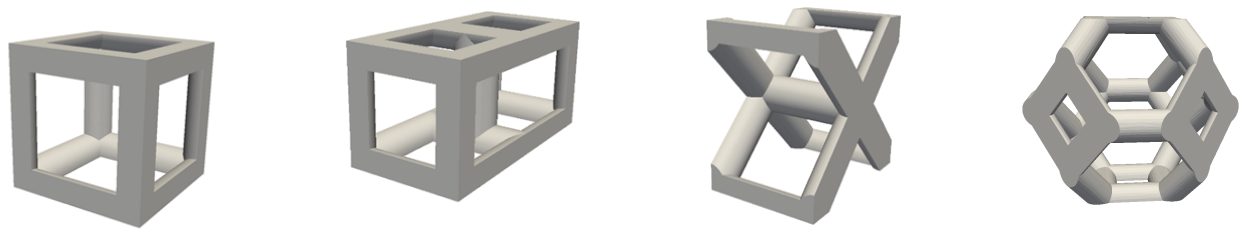

Cubic Staggered Cubic Inclined Cubic Kelvin

Figure 1: Unit Cells in POCS

Hence, the geometry of the POCS heavily influence the pressure drop and heat transfer properties and these properties have been studied experimentally as well as numerically using CFD simulations. Although there have been many studies on understanding and developing correlations for pressure drop and heat and mass transfer in POCS considering the porosity as well as the unit cell type [5], [6], only a few studies have focused on the effect of the strut shape on these properties. [8] discusses the effect of strut shape on the pressure drop properties in Kelvin cells along with a generalized pressure drop correlation which accounts for the strut shape. In [1], the effect of the strut shapes which commonly occur in manufacturing of open cellular foams on the pressure drop and convective heat transfer are studied. [2] presents the variation in the conductive heat transfer properties of the solid phase depending on the strut shape. Hence, in this study we further study the effect of strut shape on the pressure drop and convective heat transfer properties of POCS, considering the Kelvin unit cell.

1.1 Scope of this Study

In this study, we focus on only the Kelvin unit cell considering 3 different strut shapes: circular, square and rotated square as shown in Fig 2. We fix the strut dimension to 0.64 mm for all further analysis which is the diameter in case of the circular struts and the side length in case of the square and rotated square struts.

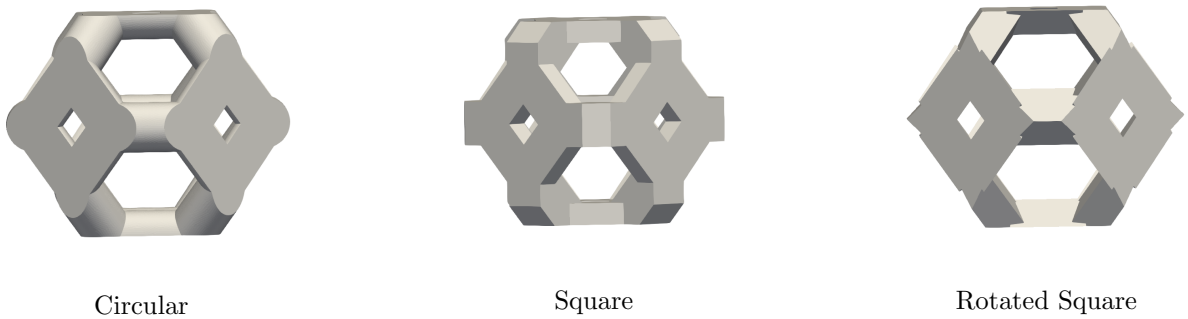

Circular Square Rotated Square

Figure 2: Kelvin Cells with different strut shapes

Further, we investigate the applicability the superposition approach proposed by [4] and [3] to the Kelvin cell with different strut shapes. The superposition approach uses the properties of individual strut arrangements to describe the properties of the entire unit cell. This approach significantly reduces the computational cost to determine the properties of POCS. Considering only the steady, laminar flow regime with hydrodynamically and thermally developed flow, a simulation with periodic boundary conditions is setup in OpenFOAM.

2 Geometry

2.1 Determination of Cell Dimension

With respect to geometrical characteristics of POCS, there are only 2 degrees of freedom. Several parameters such as the the strut diameter, porosity, specific surface area, strut length, cell length, etc. can be specified. But, only 2 of these parameters need to be fixed in order to completely describe the unit cell. In this study, the geometry is generated using a SALOME98 script which uses the strut diameter and the cell length as the input. Here we define the strut diameter d_s as the width of the strut in the direction perpendicular to the flow which is the Y direction given the flow is in X direction. Hence, for circular and square strut shapes $d_s = 0.64$ mm and for rotated square struts, $d_s = 64\sqrt{2}$ mm.

Hence, to generate unit cells with a target porosity, we fix the strut diameter and calculate the required cell dimension using geometric models proposed by [8]. The equations for the square strut shape are given below. The non linear equation 6 is solved for d_c by fixing the strut diameter and the target porosity using fsolve in MATLAB. Details of equations for other strut shapes can be found in [8].

$$L = d_c/2\sqrt{2} \tag{1}$$

$$R_{eq} = \frac{A_s}{\sqrt{\pi}}, \text{ where } A_s \text{ is the strut side length} \tag{2}$$

$$1.6R_{eq} + L_s = L, \text{ where } L_s \text{ is the strut length exluding the nodes} \tag{3}$$

$$\chi = \frac{L_s}{L} \tag{4}$$

$$\alpha = \frac{A_s}{L} \tag{5}$$

$$12\alpha^2\chi + \frac{32}{3\sqrt{\pi}}\alpha^3 = 8\sqrt{2}(1-\psi) \tag{6}$$

The results of the above procedure are tabulated below and are used subsequently for the geometry generation. For the circular strut shape, a similar model from [5] has been used which provides better results.

Strut Shape	Target Porosity	Cell Dimension (mm)	Actual Porosity (ψ)	Error (%)
Circular	0.6	219.59	0.621	3.500
	0.65	238.66	0.666	2.462
	0.7	261.91	0.712	1.714
	0.75	291.7	0.759	1.200
	0.8	331.65	0.806	0.750
	0.85	389.68	0.854	0.471
	0.9	484.84	0.901	0.111
Square	0.6	247.85	0.623	3.833
	0.65	269.28	0.668	2.769
	0.7	295.52	0.713	1.857
	0.75	328.64	0.759	1.200
	0.8	374.22	0.807	0.875
	0.85	439.5	0.854	0.471
	0.9	548.94	0.902	0.222
Rotated Square	0.6	247.85	0.617	2.833
	0.65	269.28	0.663	2.000
	0.7	295.52	0.710	1.429
	0.75	328.64	0.756	0.800
	0.8	374.22	0.805	0.625
	0.85	439.5	0.853	0.353
	0.9	548.94	0.901	0.111

Table 1: Calculated Cell Dimensions vs Porosity

The calculated cell dimensions for the square and rotated square struts are equal because the size of the strut remains same although there are slight differences in the actual porosity of the generated unit cell which is because of the geometry generation method.

2.2 Cell Geometry Generation

The Kelvin unit cell is generated using the Salome98 software. Based on the strut shape and dimension, first the cross section of the strut is created. In the next step the struts are generated and positioned appropriately. Further, the generated shape is truncated with a cube to create a single unit cell which is then multiplied or inclined based on the required geometry . After this a surface mesh is generated for the unit cell in Salome98. This procedure is outlined in the figure below which ultimately produces a STL file with the unit cell geometry.

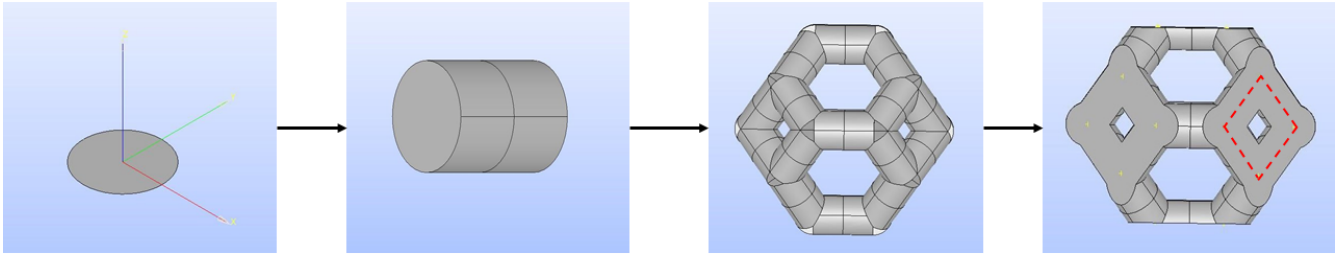

Figure 3: Unit cell generation in Salome98

In the unit cell, it is observed that the square windows highlighted in Fig 3 are the smallest. The unit cell can be generated successfully only if the struts do not completely overlap on each other. This is possible only if the strut length L is greater than the strut diameter d_s. This condition, in terms of the varied parameters d_c and d_s can be expressed as $d_{c,min} = 2\sqrt{2}d_s$.

Strut Shape	d_s (mm)	$d_{c,min}$ (mm)
Circle	64	181.02
Square	64	181.02
Rotated Square	$64\sqrt{2}$	256

Table 2: Critical Cell Dimensions

Based on the this critical cell dimension, it is evident that the the kelvin cell with rotated square struts and porosity 0.6 cannot be generated. Apart from this, the cases of circular struts with porosity 0.6 and 0.65 cannot be generated as well (even though d_c is greater than the minimum) due to the overlap of the struts caused by the custom meshing algorithm which will be discussed in the next section

This concludes the generation of the unit cell which is the solid phase which acts as a wall and is not modelled for heat transfer as we focus only on the convective heat transfer properties of the fluid flow.

2.3 Mesh Generation

For CFD simulations, we need to generate a mesh in the domain around the unit cell through which the fluid flows. For this, we use the SnappyHexMesh utility in OpenFOAM which works as follows and is also outlined in the figure below:

- Generation of a background or base mesh
- Geometry definition
- Generation of a Castellated mesh or Cartesian mesh
- Generation of a snapped mesh or body fitted mesh
- Addition of layers close to the surfaces or boundary layer meshing
- Check mesh quality

The background mesh is created using the blockMesh utility with the required dimensions of the domain. For simulations of POCS, it has been shown through domain size studies that two unit cells in the flow direction are sufficient for steady state, periodic simulations. The number of grid points in the mesh are determined from previously done grid independence studies.

The geometry is generated as a STL file as described in the previous section. Now, the external or background mesh is modified such that it is snapped onto the surface of the geometry. Further, mesh layers are added near the geometry surface to capture near wall effects

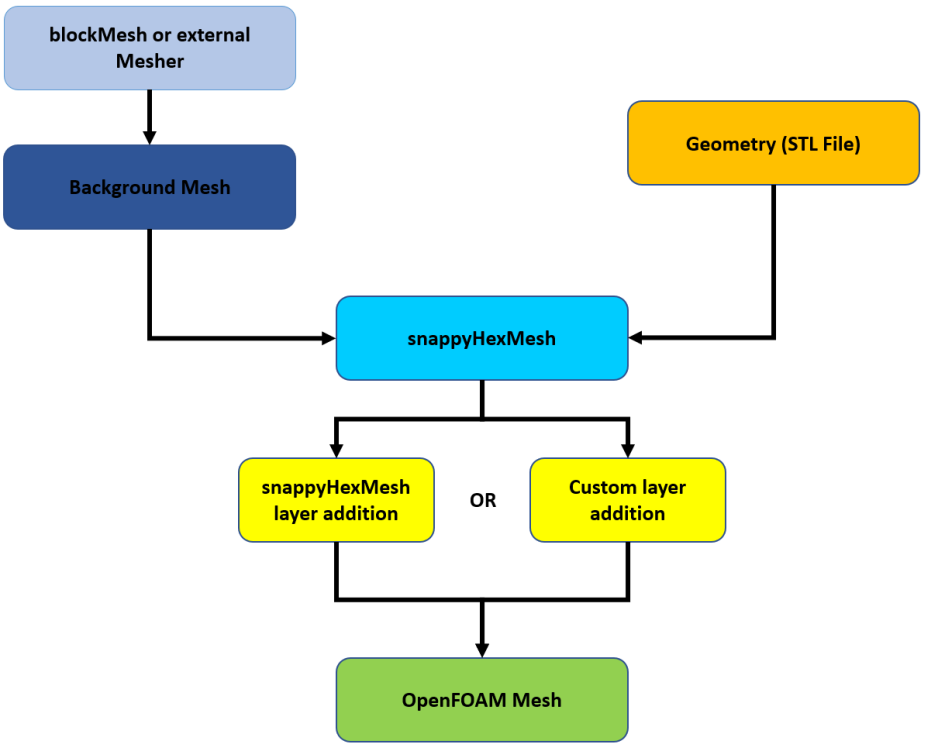

Figure 4: Steps involved in mesh generation using SnappyHexMesh

For the square and rotated square shapes, the boundary layers are added using SnapyHexMesh as described above. But, using the same procedure for the kelvin cell with circular struts gives a poor mesh quality, hence a custom layer meshing algorithm is used. In this process, the layer thickness is added to the STL geometry and the boundary layer cells are generated from this extra thickness. Due to this, the geometries for porosity 0.6 and 0.65 for the circular struts shapes were not generated as the struts overlap on the square window because of this added thickness which otherwise would be be possible if the custom meshing procedure was not used.

3 Numerical Setup

3.1 Simulation Details

Once the mesh is ready with an acceptable quality, the case is set up where we define the physical properties, boundary conditions and choose an appropriate solver for the simulation.

Water is chosen as the working fluid for the simulations with the following physical properties at 32^oC:

Property	Value	Units
Dynamic Viscosity	7.644×10^{-4}	$Pa \cdot s$
Prandtl Number	5.175	Dimensionless
Specific Heat Capacity	4180	$J/(kg \cdot K)$
Thermal Conductivity	0.6174	$W/(m \cdot K)$
Density	995.03	kg/m^3

Table 3: Physical properties of water used for the simulation

The buoyantBoussinesqSimpleFoam solver which is a steady state solver is used with second order discretization schemes. The top, bottom, left and right boundaries are defined with periodic boundary conditions for all variables. At the walls, the temperature of the unit cell is fixed as 313.15 K and for the velocity, pressure the no slip and Neumann boundary conditions are used respectively. The periodic boundary conditions on the front and the back faces of the domain which are normal to the flow directions are not trivial to define. They need to be defined in a way such that a pressure gradient is maintained across the flow direction to ensure the flow and a temperature difference is maintained to achieve heat transfer. For this, the following boundary conditions are used as given by [4]

$$u_{inlet} = u_{outlet} \tag{7}$$

$$P_{inlet} = P_{outlet} + \Delta P \tag{8}$$

$$T_{inlet} = (T_{outlet} - T_{wall}).\phi + T_{wall} \tag{9}$$

For a hydrodynamically developed flow, the velocity profile becomes constant along the flow direction hence, equation 7 is obtained. To account for the pressure drop in the periodic boundary condition, equation 8 is used. For a thermally fully developed flow, the temperature profile does not vary in the direction of the flow. This can be represented using the equation below for the non dimensional temperature profile

$$\frac{\partial}{\partial x}\left(\frac{T - T_{wall}}{T_{mean} - T_{wall}}\right) = 0 \tag{10}$$

Here, T_{mean} is the mean fluid temperature at a given axial location. Now applying this condition for the inlet and outlet, we get

$$\frac{T_{inlet} - T_{wall}}{T_{mean,inlet} - T_{wall}} = \frac{T_{outlet} - T_{wall}}{T_{mean,outlet} - T_{wall}} \tag{11}$$

As the mean fluid temperatures at the inlet and outlet are constants, the above equation can be rearranged to obtain equation 9 where the constant is taken as ϕ

The values of ϕ and ΔP need to be set such as to obtain a desired mean fluid velocity and temperature. These values are not known a priori because of the complex flow geometry, hence these values are calculated iteratively during the simulation. This boundary condition is implemented by modifying the fixedJump boundary condition in OpenFOAM. These boundary conditions are also depicted in Fig 5 taken from [4].

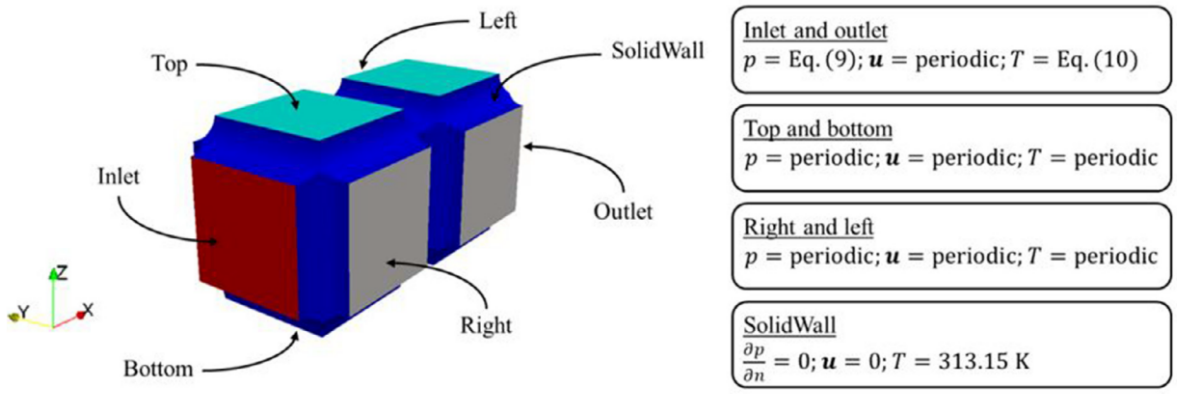

Figure 5: Boundary conditions for the periodic simulation

Properties such as the mean velocity, pressure drop, heat transfer coefficient, porosity, mean temperature, etc. are calculated during the post processing using the swak4foam library. The properties are calculated over a inner cell which spans from the center of the first cell to the second to eliminate any entrance effects if any.

3.2 Validation of the simulations

Although this setup has been validated in detail in [4] and [3] for various unit cell types, we still present 2 cases for validation with the Kelvin cell, one for the pressure drop and one for the convective heat transfer coefficient.

For the pressure drop, we compare the simulation results for the circular strut shape with the correlation from [6] which is given as below:

$$-\nabla P = A \cdot \frac{\mu}{\phi d_{window}^2} \cdot u_0 + B \cdot \frac{\rho}{\phi^2 d_{window}} \cdot u_0^2 \tag{12}$$

$$A = 6.28, \quad B = 0.29$$

$$d_{window} = \sqrt{\frac{(d_c - 2d_s)(d_c - 2\sqrt{d_s})}{6}}$$

Fig 6a shows the comparison of the simulation results and the correlation. The average mean percentage error between the two is 5.997% which is acceptable

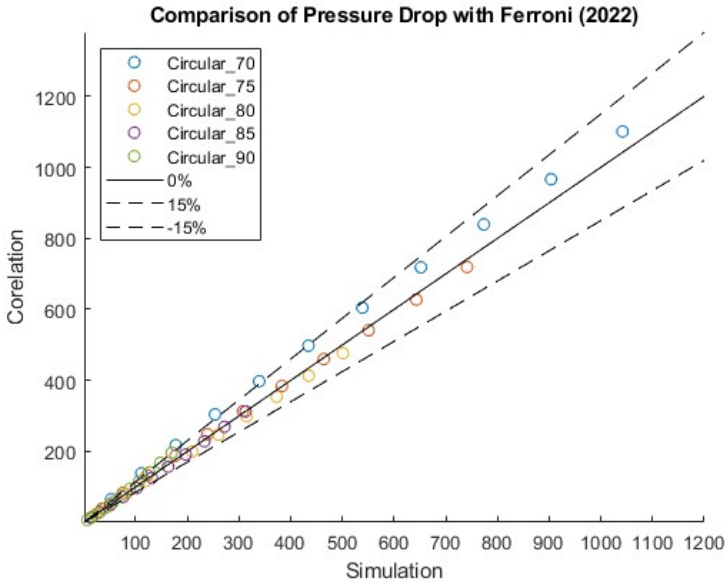

(a) Validation of pressure drop

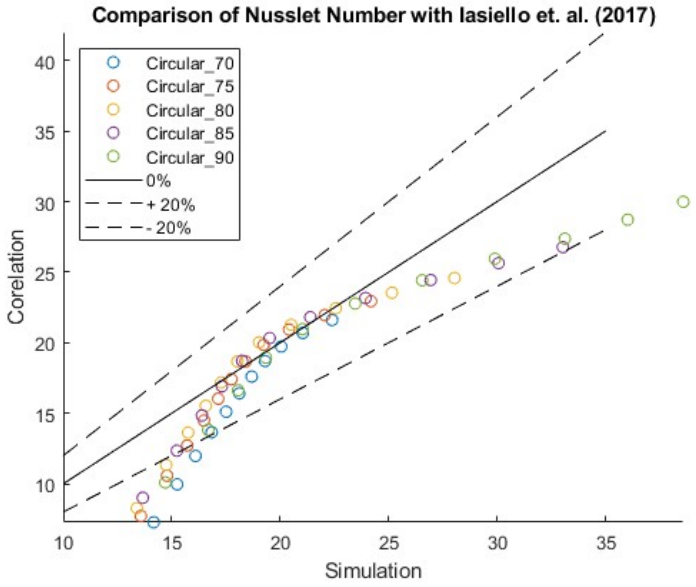

(b) Validation of Nusselt number

Figure 6: Comparison of simulation data with correlations in literature

To validate the solver for heat transfer properties, we use the correlation from [7] which is given as follows:

$$Nu = 1.594 Re^{0.454} \psi^{0.1644} \tag{13}$$

$$Nu = \frac{h d_c}{\psi \lambda}; \quad Re_D = \frac{u_0 d_c}{\psi \nu}$$

As the above as calculated considering air as the working fluid while we use water, an extra term related to the Prandtl number is added to account for the change in the fluid and the corrected equation is given as below

$$Nu = 1.594\, Re^{0.454}\, \psi^{0.1644} \left(\frac{Pr_{\text{water}}}{Pr_{\text{air}}} \right)^{\frac{1}{3}} \tag{14}$$

The results show a mean average percentage error of 12.12%. This error is higher at lower velocities as seen in Fig 6b, but overall the error is under an allowable limit. This could be because of the geometry considered in [7] being slightly different in the sense that the windows in the Kelvin cell are more rounded. The effect of this change in geometry is evident at lower velocities compared to higher velocities which are dominated by inertial effects. Another reason for the observed deviations might be because [7] uses constant heat flux wall boundary conditions while we have use constant wall temperature boundary condition for the simulations.

Thus we can conclude that the solver is validated using correlations from the literature and can be used for analysis of further cases.

4 Hydrodynamics

4.1 Characteristics of Pressure Drop

As expected, for each of the struts shapes, at a given porosity, the pressure drop increases with the velocity. At a fixed velocity, the pressure drop decreases with the porosity.

It is observed that the pressure drop vs velocity variation has 2 regimes which are plotted in Fig 7d. In some literature [9] another regime has been distinguished between the two described above which is the transitional regime. This regime shows a cubic velocity dependence but only for a narrow range of velocities, hence we do not analyze this regime further in this section. As the linear regime occurs at very low velocities, the velocity is plotted in a log scale to clearly distinguish between the two regimes.

$$-\frac{\Delta P}{L} = \frac{\mu}{\kappa} v \tag{15}$$

$$-\frac{\Delta P}{L} = \frac{\mu}{\kappa} v + \beta \rho v^2 \tag{16}$$

The first regime which we call Regime 1 is the Darcy Regime or the linear regime where the pressure drop varies linearly with the velocity as given in equation 15 which is the Darcy's Law. In this regime, the flow is dominated by viscous effects. The second regime which we call as Regime 2 is governed by the a quadratic law also known as the Forcheimmer equation given in equation 16. In this regime, the flow is dominated by inertial effects, hence the first term in the equation 16 is the viscous term and the second term is the inertial term. The linear coefficient κ is known as the Darcy Permeability and the quadratic coefficient β is called as the Inertia Coefficient. In some cases, where the cubic regime is also considered, Regime 2 is the cubic regime and Regime 3 is the quadratic regime, but for the following analysis, we consider these two as a single regime and call it Regime 2 For the case of circular struts with porosity 0.8 in Fig 7d, these values are calculated by curve fitting as $\kappa = 7.7593.10^{-8}\ m^2$ and $\beta = 449.99\ m$

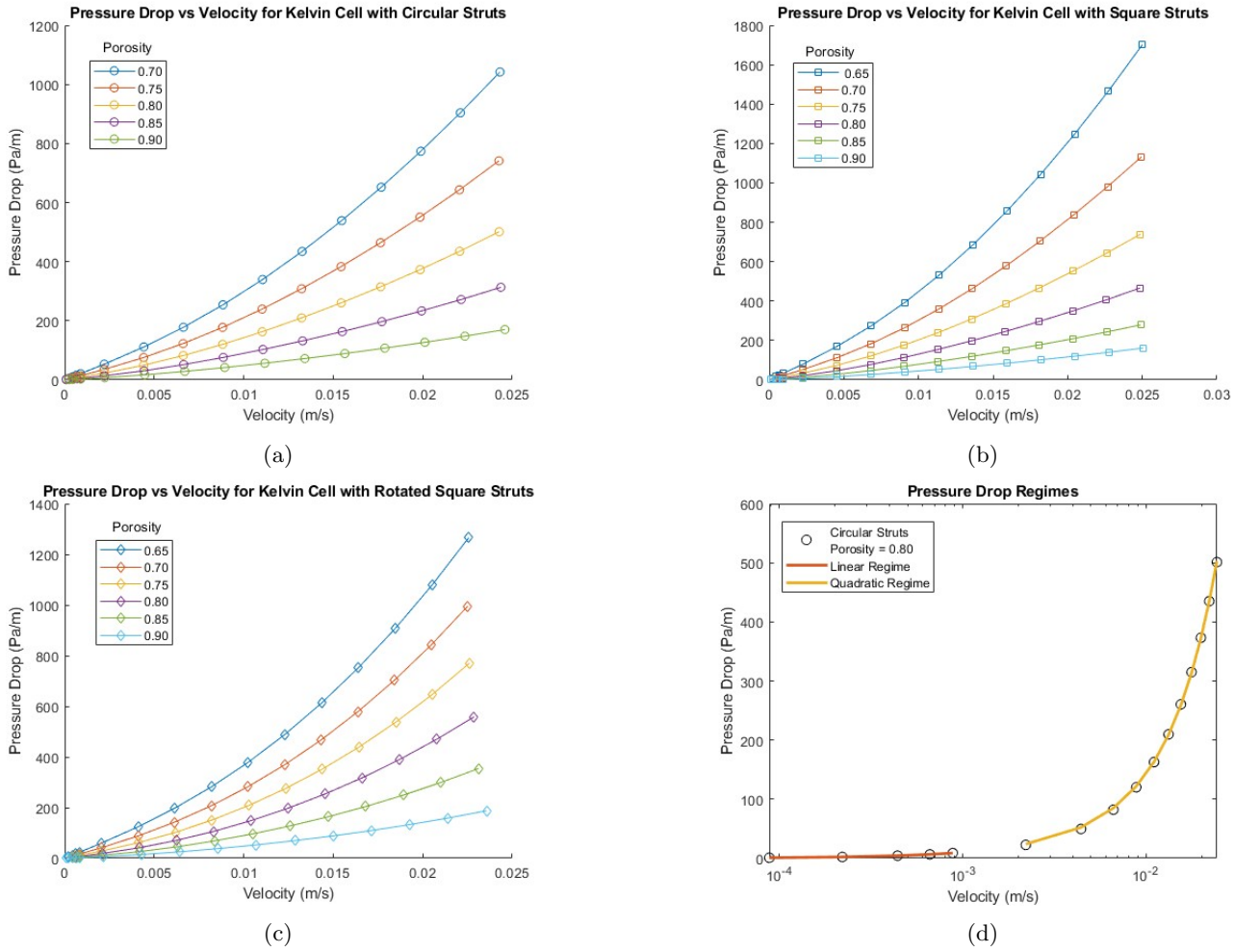

Figure 7: Pressure Drop vs Velocity for different strut shapes

In non dimensional form, equation 16 can be expressed in terms of the Reynolds number and the Hagen number as given in equation 17. The Hagen number comes up naturally while converting the Forchhemier equation to a non dimensional form, we use this dimensionless number for further analysis and comparison of different strut shapes.

$$Hg = Re.\frac{L_{char}}{\kappa} + Re^2.\beta.L_{char} \tag{17}$$

$$Hg = -\frac{\Delta P}{L}\frac{\rho L_{char}^3}{\mu^2}; \quad Re = \frac{\rho v L_{char}}{\mu} \tag{18}$$

4.2 Comparison of different Strut Shapes

In this section we compare the Hagen vs Reynolds number variation at a fixed porosity for different strut shapes. As given in equation 18, we need a characteristic length scale to define these non dimensional quantities. [3] states that there are various ways of defining the length scale for POCS. Some of the previously used length scales include the strut dimension d_s, the cell diameter d_c, semi perimeter of the strut, hydraulic diameter and a Darcy Permeability based length scale. We have compared the variation of the non dimensional properties for each strut shapes with each of the above mentioned length scales. In this section, results using 2 of the length scales which produce different results are presented. Using different characteristic length scales can lead to the development of generalized correlations independent of the strut shape.

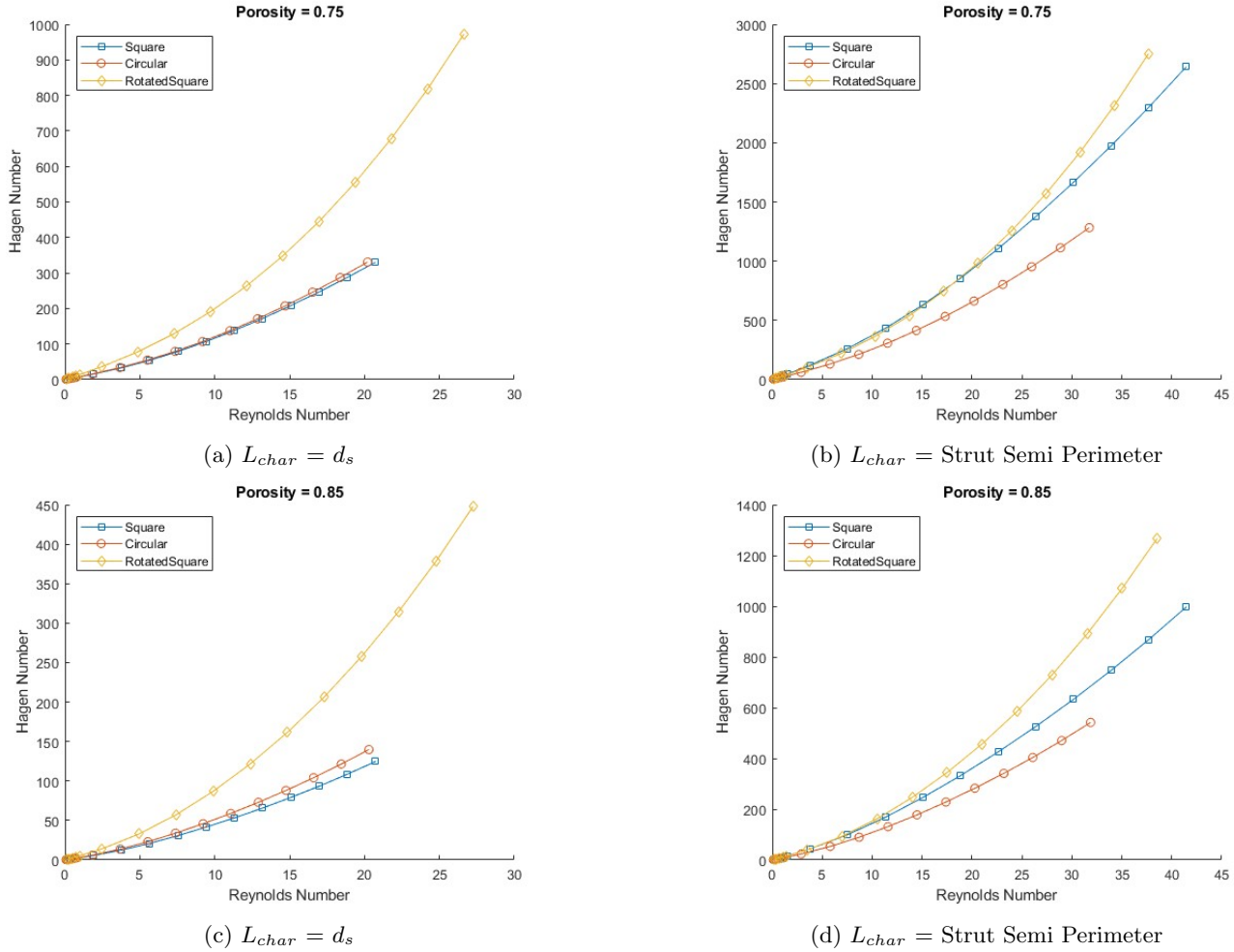

(a) $L_{char} = d_s$

(b) L_{char} = Strut Semi Perimeter

(c) $L_{char} = d_s$

(d) L_{char} = Strut Semi Perimeter

Figure 8: Hg vs Re comparison using different length scales

Fig 8a and 8c show the Hg vs Re variation when the strut diameter is used as the characteristic length scale. The variation of the Hagen number vs Reynolds number has the same profile for all strut shapes. It is observed that at all porosities, the Hagen number follows the following trend: Rotated Square > Circular > Square. Only at the lowest porosity which is 0.7, the Hg for the square struts is slightly higher than that of the circular struts. The properties at such low porosities may not be practically relevant for heat transfer applications due to the significantly higher pressure drop values. As d_s is equal for the circular and square struts, we can also conclude that the pressure drop for the circular struts is also greater than that for the square struts at any given velocity.

The range of Reynolds numbers in each strut shape is also different even though the investigated velocities are the same because of the length scales being dependent on the strut shape.

When the strut semi perimeter is used as the characteristic length scale, we have $L_{char} = \frac{\pi d_s}{2}$ for the circular struts and for the square and rotated square struts, $L_{char} = 2d_s$. Using this characteristic length scale, we obtain the plots in Fig 8b and 8d . As expected, the trend in the Hg vs Re for different strut shapes still remains the same. The comparison between the square and rotated square strut shapes is the same as the actual pressure drop vs velocity variation because the characteristic length is same for both the cases. Using this length scale, the similarity between the characteristics of the square and rotated square strut shapes can be clearly seen, especially in the Darcy regime. Again, only at the lowest porosity, the kelvin cell with square struts has a higher Hagen number than that for the rotated square struts.

5 Heat Transfer

5.1 Characteristics of Convective Heat Transfer

The large specific area of POCS leads to comparatively high heat transfer coefficients which is why they find a lot of applications in the area of heat transfer. In general, the heat transfer coefficient increases with the velocity and as expected this is observed in Fig 9 at a fixed porosity for all strut shapes. The heat transfer coefficient increases with decreasing porosity as the maximum fluid velocity and the solid surface area increases.

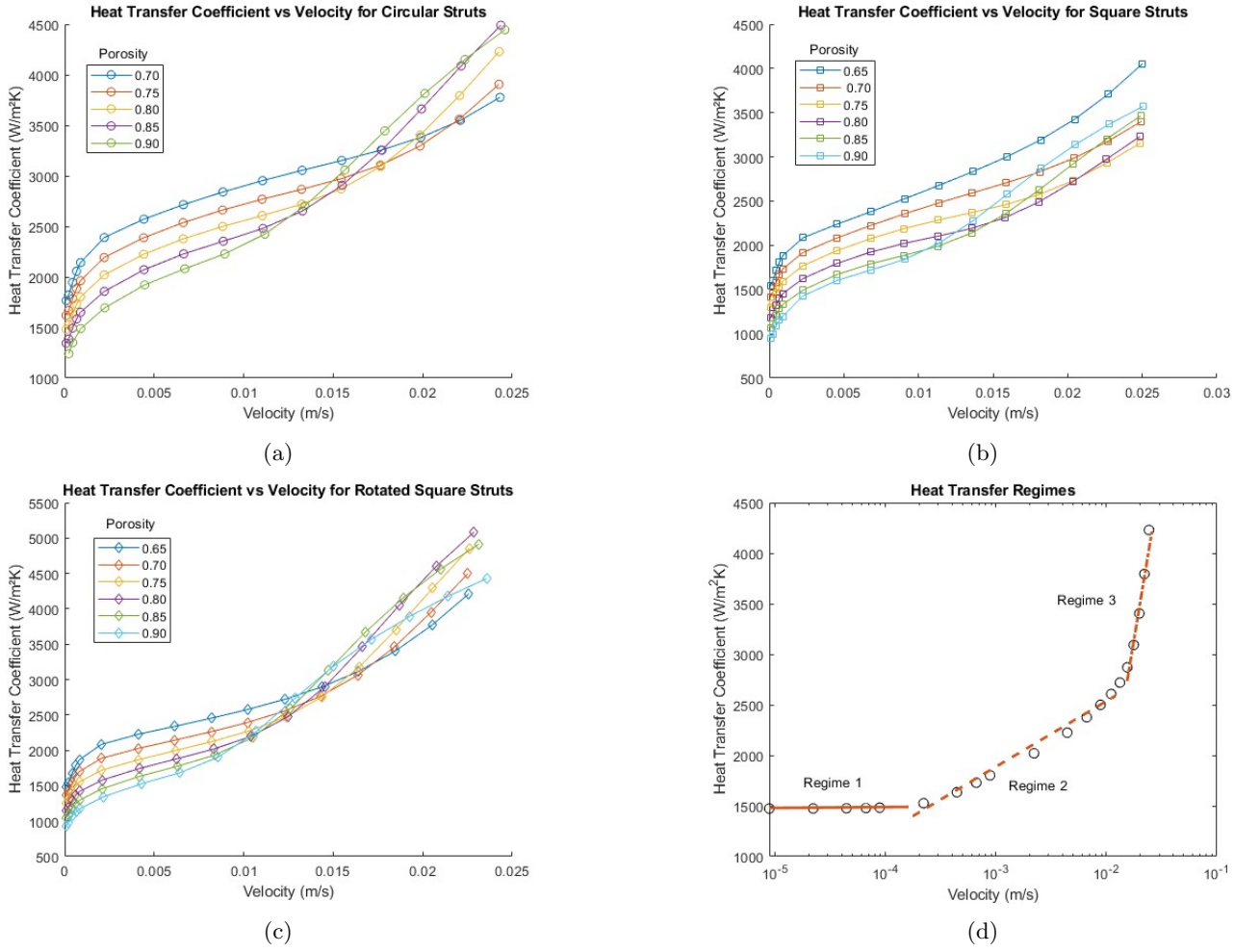

Figure 9: Heat Transfer Coefficient vs Velocity for different strut shapes

There are three regimes which can be distinguished from Fig 9 for each strut shape. Considering a few more lower velocity cases for the case of circular struts with porosity 0.8 as shown in Fig 9d, we can observe the 3 regimes more clearly when the velocity is plotted in log scale. In regime 1, the heat transfer coefficient is independent of the velocity, which occurs only at very low velocities. In this regime, the heat transfer is dominated by conduction and the entire unit cell is filled by the boundary layer. As the velocity increases, the boundary layer thickness reduces, the heat transfer coefficient depends on the velocity and the deflection of the flow due to the struts. In regime 3, the slope of the heat transfer coefficient vs velocity further increases because of formation of stationary re-circulation zones in the wake of the struts. The transition from Regime 1 to 2 occurs at around the same velocity

for all porosities. But the transition from Regime 2 to 3 is highly dependent on the porosity, occurring at relatively low velocities at higher porosities. When comparing the different strut shapes in Fig 9a - 9c it can be seen that the curves are similar to each other at lower flow velocities, but the behaviour then differs at higher flow velocities depending on the strut shape. The influence of the strut shape is discussed in more detail in the following section

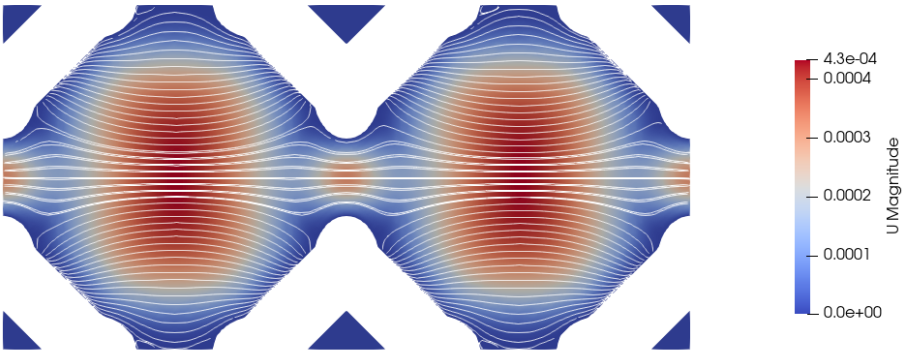

(a) v = 0.00025 m/s, Re = 0.2886

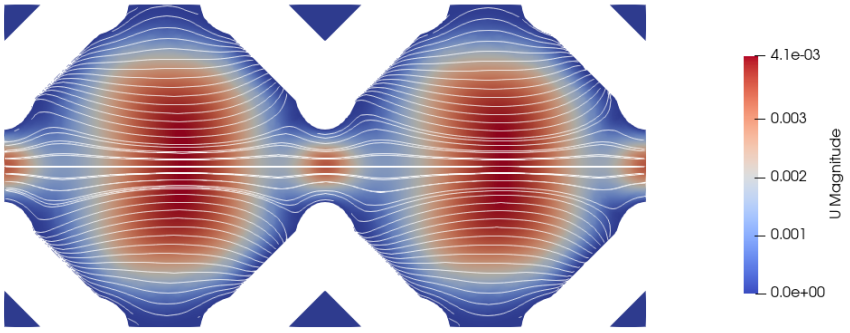

(b) v = 0.0025 m/s, Re = 2.886

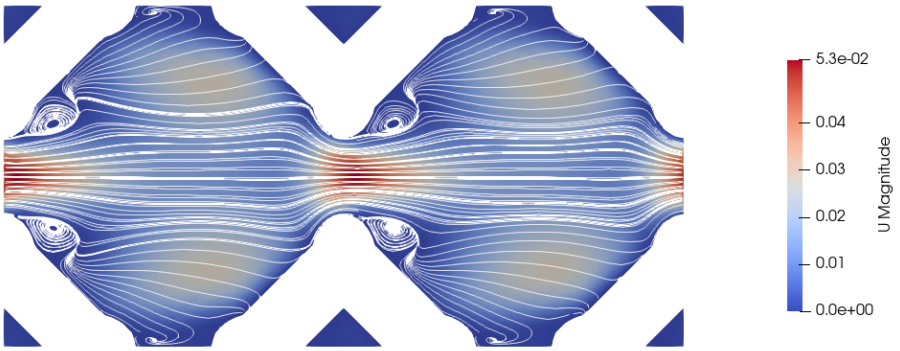

(c) v = 0.025 m/s, Re = 28.86

Figure 10: Velocity contours and streamlines for the Kelvin cell with circular struts with porosity 0.8

These characteristics are also visible in Fig 10 which shows the streamlines plotted along with the streamlines. The flow in Regime 1 is symmetric and viscous dominated where the Nusslet number remains constant. In Regime 2 the velocity distribution starts to show asymmetry, moving into the inertial regime where the Nusselt number starts showing a dependence on the Reynolds number. In Regime 3, re-circulation zones are observed which promotes the fluid intermixing, enhancing the Nusselt number.

5.2 Comparison of different Strut Shapes

For the non dimensional analysis of the heat transfer, we use the Nusselt number which is defined as $Nu = \frac{hL_{char}}{k}$. Again there are several options for the choice of the length scale. Further, we only consider two cases of the characteristic lengths as before which are the strut diameter and semi perimeter.

Using the strut diameter as the characteristic length scale, we observe that the Nusselt number for the Rotated Square struts is the highest followed by the circular and square struts. This is the same order as observed for the Hagen number which implies that even though the rotated square struts provide better convective heat transfer, at the same time the pressure drop is higher compared to other strut shapes. The curves follow the same trends in Regime 1 and 2 irrespective of the strut shape. The regime transitions also seem to be independent of the strut shape at any given porosity. But in Regime 3, the variation becomes strut shape dependent as the slope of the curve is highest for the rotated square struts and the lowest for the square struts.

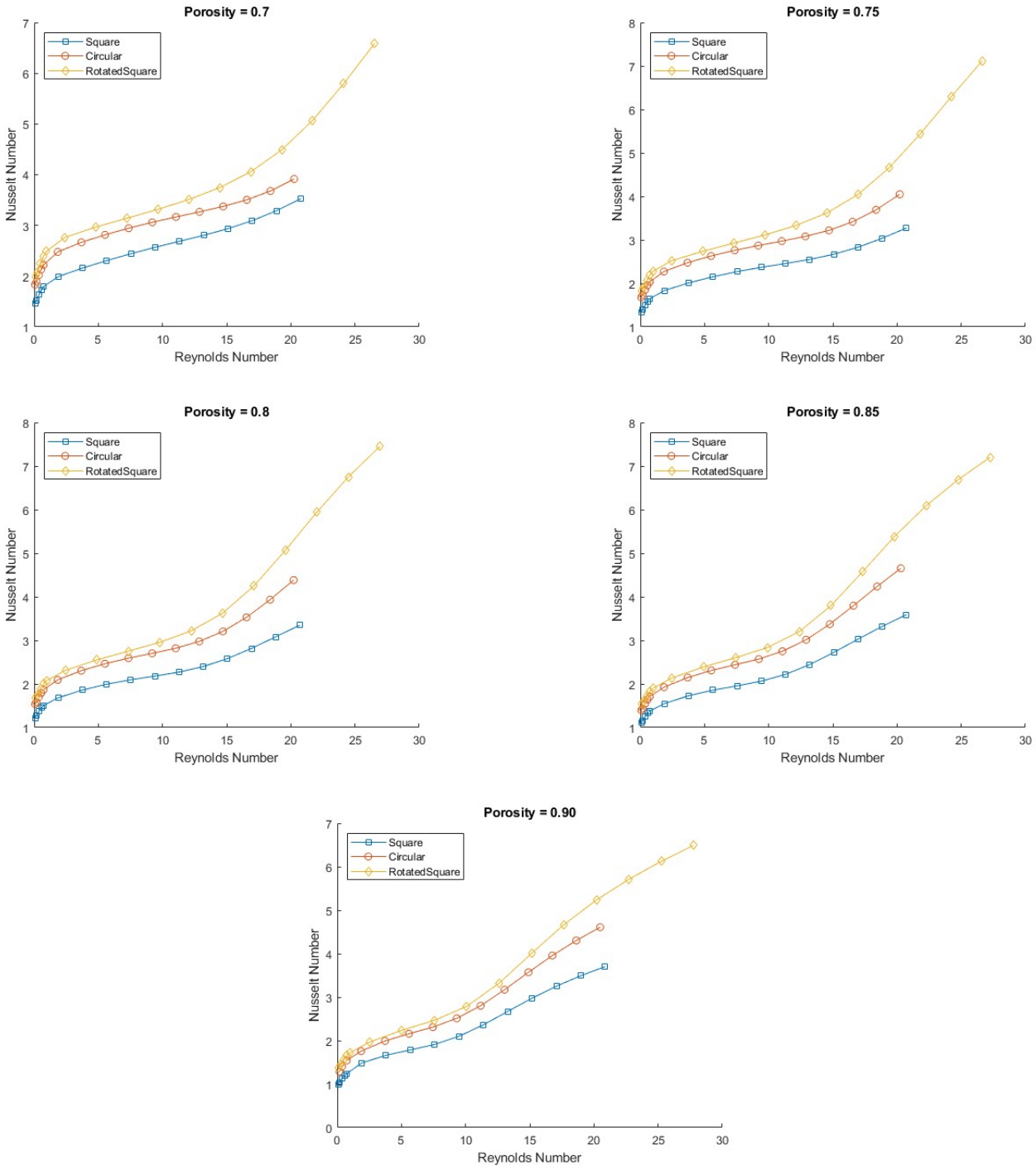

Figure 11: Nu vs Re comparison using $L_{char} = d_s$

Using the strut semi perimeter as L_{char}, there are some interesting observations from Fig 12. Few characteristics remain same as concluded previously - Nusselt number at any given porosity follows the trend - Rotated Square $>$ Circular $>$ Square, the slope of the curves in Regime 3 also follow the same order and the transition to Regime 3 occurs at a lower Re at higher porosities. But, the curves in Regime 1 and 2 for all strut shapes coincide for each porosity, which gives a set of curves of Nu vs Re which are independent of the strut geometry.

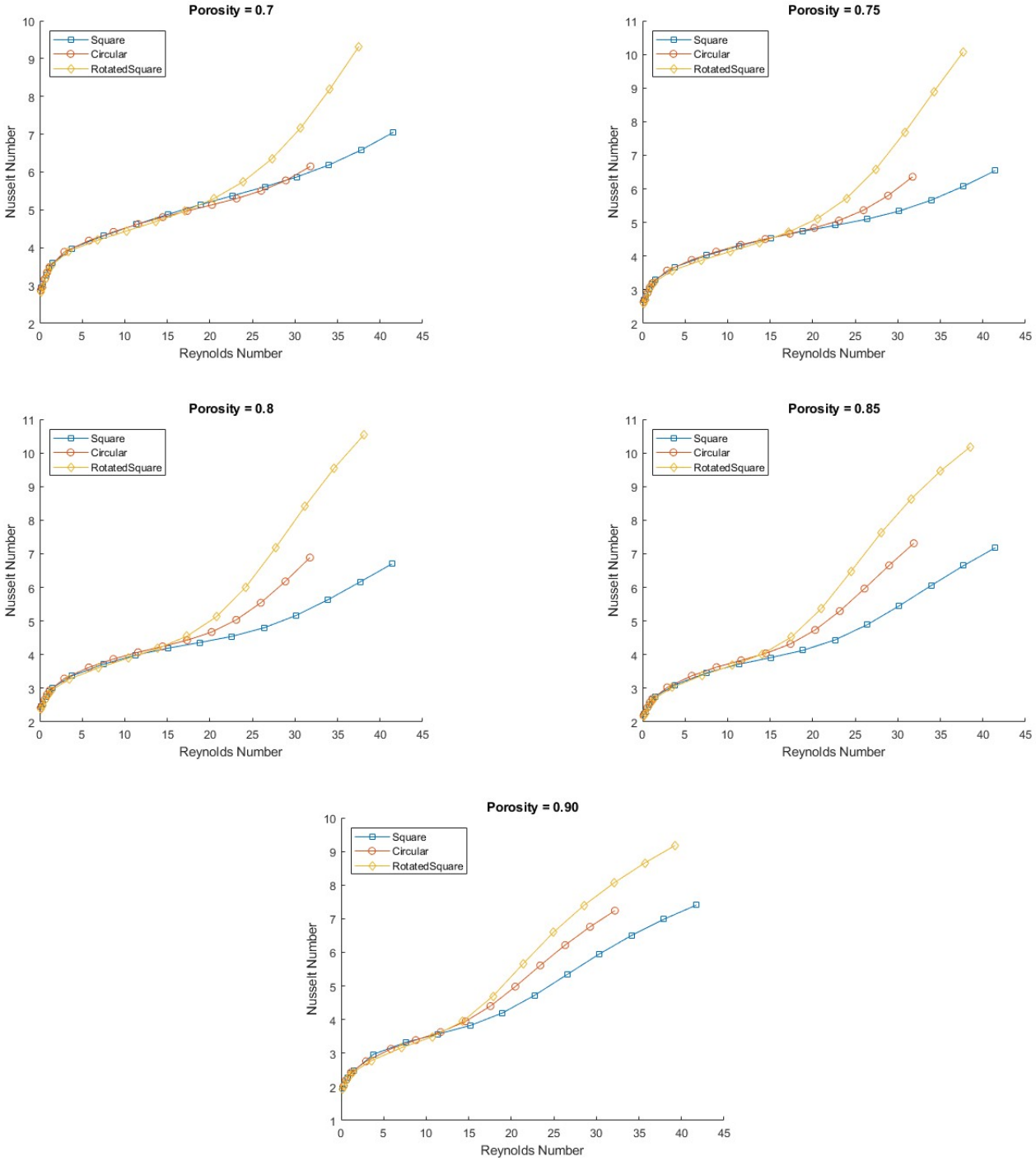

Figure 12: Nu vs Re comparison using L_{char} = Strut Semi Perimeter

6 Superposition Approach

6.1 Methodology

In this section, the superposition approach as proposed by [3] is described and later applied to the Kelvin cell POCS considering the different strut shapes. The key idea behind this approach is the question - Can the properties of the unit cell be described by a superposition by the individual strut arrangements which make up the unit cell? Using such an approach to determine the properties of POCS would reduce the associated computational cost as simulations of strut arrangements are cheaper and can be reused for various unit cell geometries.

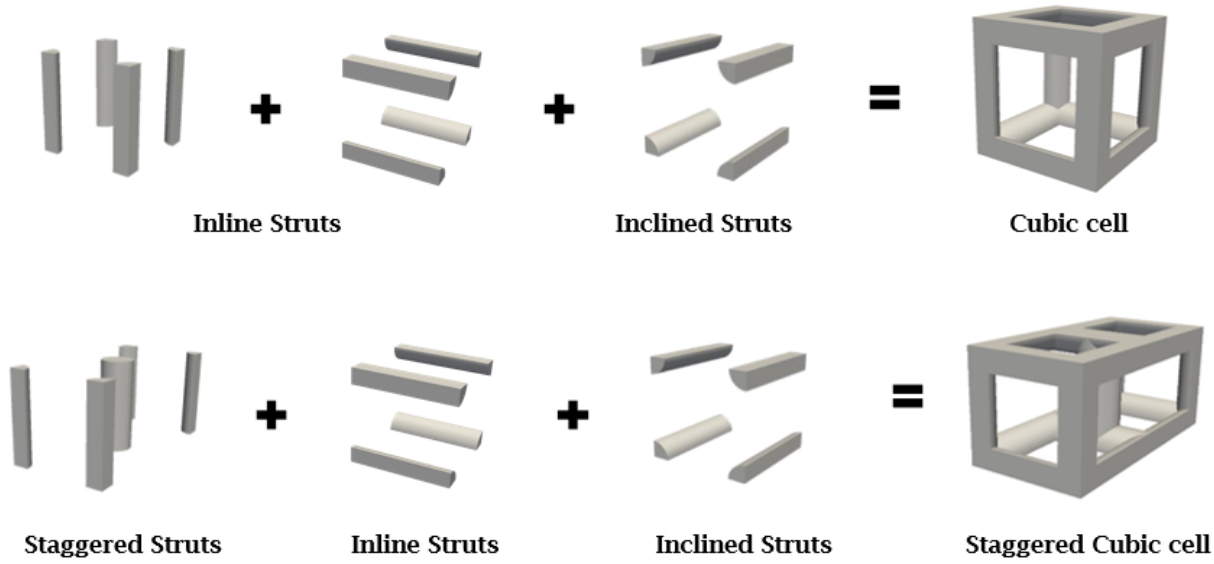

Figure 13: Superposition applied to the cubic unit cell

This idea is depicted in Fig 13, for simple cases of the cubic and staggered cubic cells. Here, strut arrangements refer to the positioning of struts similar to tube banks which have been studied in literature for their applications in shell and tube heat exchangers. The strut arrangements are further divided into 3 categories:

- Inline Struts (F struts) - Inline Struts are the type of struts which experience cross flow. It has been shown that the hydrodynamic and heat transfer properties of such struts do not depend heavily on their orientation as long as they are not aligned along the flow direction. Hence, all such struts which are at an angle to the flow come under this category
- Inclined Struts (Y Struts) - These struts are aligned with the direction of flow and hence are distinguished from the inline struts as there is a change in the properties when the struts are oriented along the flow. The flow through these struts is a channel like flow which does not induce flow deflection in contrast to the inline struts in cross flow.
- Staggered Struts (V Struts) - In staggered struts, as shown in Fig **??** consecutive rows of struts are staggered with respect to each other, in contrast to the other types of struts described above where the struts in each row are aligned with each other.

Further, the arrangement of these struts is described by two dimensionless pitches s_L and s_T which are the longitudinal and transverse pitches. This is defined in Fig 14 with the top views of the inline and staggered struts and the front view of the inclined strut arrangement. These pitches are also defined for the unit cells and for the Kelvin Cell, $s_T = s_L = \frac{d_{cell}}{d_{strut}}$. The pitches of the strut arrangements are derived from their respective unit cells. Table 4 from [3] gives a summary of the decomposition of various unit cells, with the number of struts of each type and their dimensionless pitches.

For the Kelvin cell, this decomposition of the unit cell is not so trivial but has been derived in [3]. The Kelvin cell is constructed as a superposition of two types of inline struts (F1 and F2 struts) and one set of staggered struts (V struts). The pitches for these struts are calculated according to Table 4. Steady state, periodic simulations are then carried out for these strut arrangements using the same numerical setup as described in the previous sections for the unit cells. The results from these simulations are the then used to test the superposition approach in the following steps for both predicting the pressure drop and the convective heat transfer properties of the unit cell.

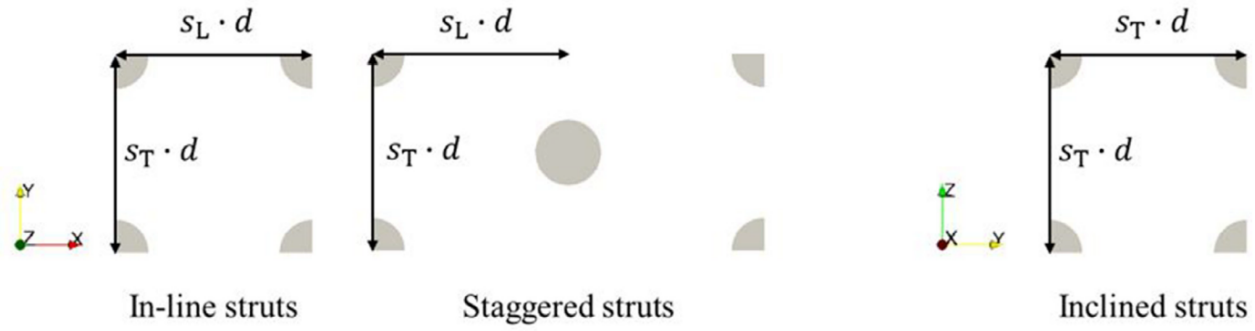

Figure 14: Dimensionless pitch definitions for each of the strut arrangements

Unit Cell Type	F Struts			V Struts			Y Struts	
	N_i	$s_{L,strut}$	$s_{T,strut}$	N_i	$s_{L,strut}$	$s_{T,strut}$	N_i	$s_{T,strut}$
Cubic	2	s_L	s_T	-	-	-	1	s_T
Staggered Cubic	-	-	-	4	s_L	s_T	2	s_T
Inclined Cubic	4	$\sqrt{2}s_L/2$	s_T	2	$s_L/\sqrt{2}$	$\sqrt{2}s_T$	-	-
Double inclined cubic	-	-	-	18	$s_L/\sqrt{3}$	$2s_T/\sqrt{6}$	-	-
Kelvin	4	s_L	$\sqrt{2}s_T/4$	10	$s_L/2$	$\sqrt{2}s_T/2$	-	-
	10	$s_L/2$	s_T	-	-	-	-	-
Diamond	-	-	-	16	$s_L/2$	$\sqrt{2}s_T/2$	-	-

Table 4: Equivalent Strut Arrangements

Pressure Drop

The Hagen number of the unit cell is expressed in terms of the strut arrangements as given by equation 19

$$Hg = \Sigma Hg_i \phi_i \ , \ \phi_i = \frac{N_i}{N} \frac{S_v}{S_{v,i}} \tag{19}$$

Here, N is the total number of struts in the equivalent strut arrangements and S_v denotes the specific surface area of the unit cell. $S_{v,i}$ is the specific surface area of the strut arrangements which are calculated as below:

$$S_{v,F} = \frac{\pi}{s_L s_T d_s} \ , \ S_{v,V} = \frac{\pi}{s_L s_T d_s} \ , \ S_{v,Y} = \frac{\pi}{s_T s_T d_s} \tag{20}$$

To calculate Hg_i, we first develop a correlation for the Hg vs Re of the strut arrangements of the form given in equation 21 using a least squares curve fit. In the superposition approach, for calculating the non dimensional quantities, we always use the characteristic length scale as the strut semi perimeter unless otherwise specified.

$$Hg = \begin{cases} B \cdot Re_{in}, & \text{Regime 1} \\ B \cdot Re_{in}^m, & \text{Regime 2 and 3} \end{cases} \quad \text{where,} \quad Re_{in} = \frac{\rho v_o L_{char}}{\mu \psi_{in}} \tag{21}$$

ψ_{in} is the inlet porosity, which is calculated as the fraction of the area available for the flow when viewed along the main flow direction. This is calculated for the Kelvin cell with all strut shape as

$$\psi_{in} = 1 - \frac{\sqrt{2}}{s_T} \tag{22}$$

The regimes in equation 21 are determined for the unit cells based on pressure drop and heat transfer data from different unit cells and porosities. The Regime boundaries in terms of the critical Reynolds number proposed by [3] are given as

$$Re_c = 7 - 6.6\psi \ \text{ between Regime 1 and 2}, \quad Re_c = 24 - 22\psi \ \text{ between Regime 2 and 3} \tag{23}$$

While deriving these coefficients B and m of equation 21 through curve fitting, we calculate the Reynolds number for the strut arrangements with a corrected average velocity, which is defined using the superficial velocity and the porosity of a single strut row as follows

$$Re = \frac{\rho v_o L_{char}}{\mu \psi_r} \ , \ \psi_r = 1 - \frac{\pi}{4 s_T} \tag{24}$$

In case of the square and rotated square struts, this porosity is calculated as $\psi_r = 1 - \frac{1}{s_T}$

Heat Transfer

The Nusselt number of the unit cell can be expressed in terms of the Nusselt number of the strut arrangements using the superposition equation given below:

$$Nu = \Sigma Nu_i \frac{A_i}{A_{cell}} \; where, \; A_i = A_{strut} \cdot N_i \cdot \phi_{node} \cdot \phi_{proj} \tag{25}$$

Here, A is the surface area of the unit cell, A_i is the surface area of the strut arrangement and A_{strut} is the surface area of a single strut which depending on the strut shape is $\pi d_s L$ for the circular struts and $2d_s L$ for the square and rotated square struts. The length of the strut L is calculated as $d_c/2\sqrt{2}$ for the Kelvin cell. For the strut arrangement, there are two extra correction factors considered which are the node factor ϕ_{node} and the projection factor ϕ_{proj}. The node factor accounts for the reduced surface area of the struts due to their intersection at the nodes as well as formation of stagnation zones near the nodes which reduce the heat transfer. An expression for the node factor has been derived by [3] considering various unit cells and porosities which is given as

$$\phi_{node} = 0.839\psi - 0.07 \tag{26}$$

The projection factor is used to consider the difference in between the inline and inclined struts which is defined as below. As the equivalent strut arrangement for the Kelvin unit cell does not consist of the inclined struts, the projection factor is simply taken as one.

$$\phi_{proj} \begin{cases} 1\ , & \text{F and V Struts} \\ \frac{2}{\pi}\ , & \text{Y Struts} \end{cases} \tag{27}$$

To calculate Nu_i, we again develop a correlation between Nu and Re for the strut arrangements by curve fitting of the form given in equation 28. The regime boundaries used here are the same as given in equation 23.

$$Nu = \begin{cases} A, & \text{Regime 1} \\ A \cdot Re^n, & \text{Regime 2 and 3} \end{cases} \quad \text{where,} \quad Re = \frac{\rho v L_{char}}{\mu} \tag{28}$$

To derive these correlations through curve fitting, in the case of Nu vs Re as well, the Reynolds number is defined in the same way as described for the Hg vs Re correlation in equation 24.

6.2 Implementation

To apply the superposition approach to the cases of the Kelvin cell with different strut shapes, we first calculate the pitches of the unit cell and the equivalent strut arrangements which are given in tables 5, 6 and 7. Each unit cell has a specific cell dimension based on the porosity as calculated in Table 1 and corresponding to each such case we have an equivalent strut arrangement for which the pitch is calculated. We consider the cases of all strut shapes from porosity 0.7 to 0.9 and including porosity 0.65 for the square strut shape. The case of 0.65 for the rotated square struts can be generated, but the cell dimension is very close to the critical cell dimension as described in Table 2 which is why the characteristics of the hydrodynamic and thermal boundary layer differ. Therefore, this case in not considered for further analysis

Porosity	**Cell Dimension (mm)**	$s_{L,cell}$	$s_{T,cell}$	**F1**		**F2**		**V**	
				s_L	s_T	s_L	s_T	s_L	s_T
0.70718	0.0025889	4.045	4.045	4.045	1.430	2.023	4.045	2.023	2.860
0.75526	0.002888	4.513	4.513	4.513	1.595	2.256	4.513	2.256	3.191
0.80365	0.0032892	5.139	5.139	5.139	1.817	2.570	5.139	2.570	3.634
0.85226	0.0038713	6.049	6.049	6.049	2.139	3.024	6.049	3.024	4.277
0.900615	0.0048262	7.541	7.541	7.541	2.666	3.770	7.541	3.770	5.332

Table 5: Equivalent strut arrangement for Kelvin cell with circular struts

Porosity	**Cell Dimension (mm)**	$s_{L,cell}$	$s_{T,cell}$	**F1**		**F2**		**V**	
				s_L	s_T	s_L	s_T	s_L	s_T
0.66797	0.0026928	4.208	4.208	4.208	1.488	2.104	4.208	2.104	2.975
0.71328	0.0029552	4.618	4.618	4.618	1.633	2.309	4.618	2.309	3.265
0.75907	0.0032864	5.135	5.135	5.135	1.815	2.568	5.135	2.568	3.631
0.80669	0.0037422	5.847	5.847	5.847	2.067	2.924	5.847	2.924	4.135
0.85394	0.004395	6.867	6.867	6.867	2.428	3.434	6.867	3.434	4.856
0.90236	0.005500	8.594	8.594	8.594	3.038	4.297	8.594	4.297	6.077

Table 6: Equivalent strut arrangement for Kelvin cell with square struts

Porosity	Cell Dimension (mm)	$s_{L,cell}$	$s_{T,cell}$	F1		F2		V	
				s_L	s_T	s_L	s_T	s_L	s_T
0.70953	0.0029552	3.265	3.265	3.265	1.154	1.633	3.265	1.633	2.309
0.75636	0.0032864	3.631	3.631	3.631	1.284	1.815	3.631	1.815	2.568
0.80477	0.0037422	4.135	4.135	4.135	1.462	2.067	4.135	2.067	2.924
0.85275	0.004395	4.856	4.856	4.856	1.717	2.428	4.856	2.428	3.434
0.90236	0.0054894	6.065	6.065	6.065	2.144	3.032	6.065	3.032	4.289

Table 7: Equivalent strut arrangement for Kelvin cell with rotated square struts

Now, the next step is to calculate the coefficients A, B, m and n for the Hagen and Nusselt number correlations using the regime boundaries and a least square curve fit using lsqcurvefit in MATLAB. Figures 16 and 17 show an example of this curve fitting for the case of the circular struts for the Hagen number and Nusselt number respectively. A general power law expression is used for curve fitting for all regimes and the results to get better fits in each regime.

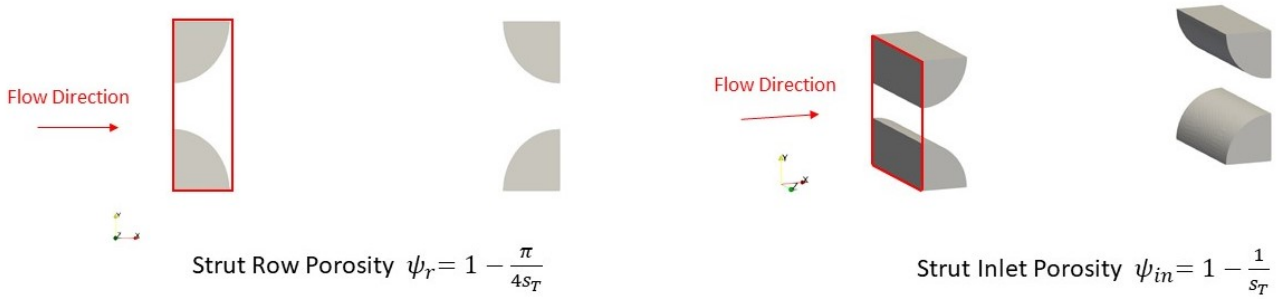

Figure 15: Porosity for strut arrangements

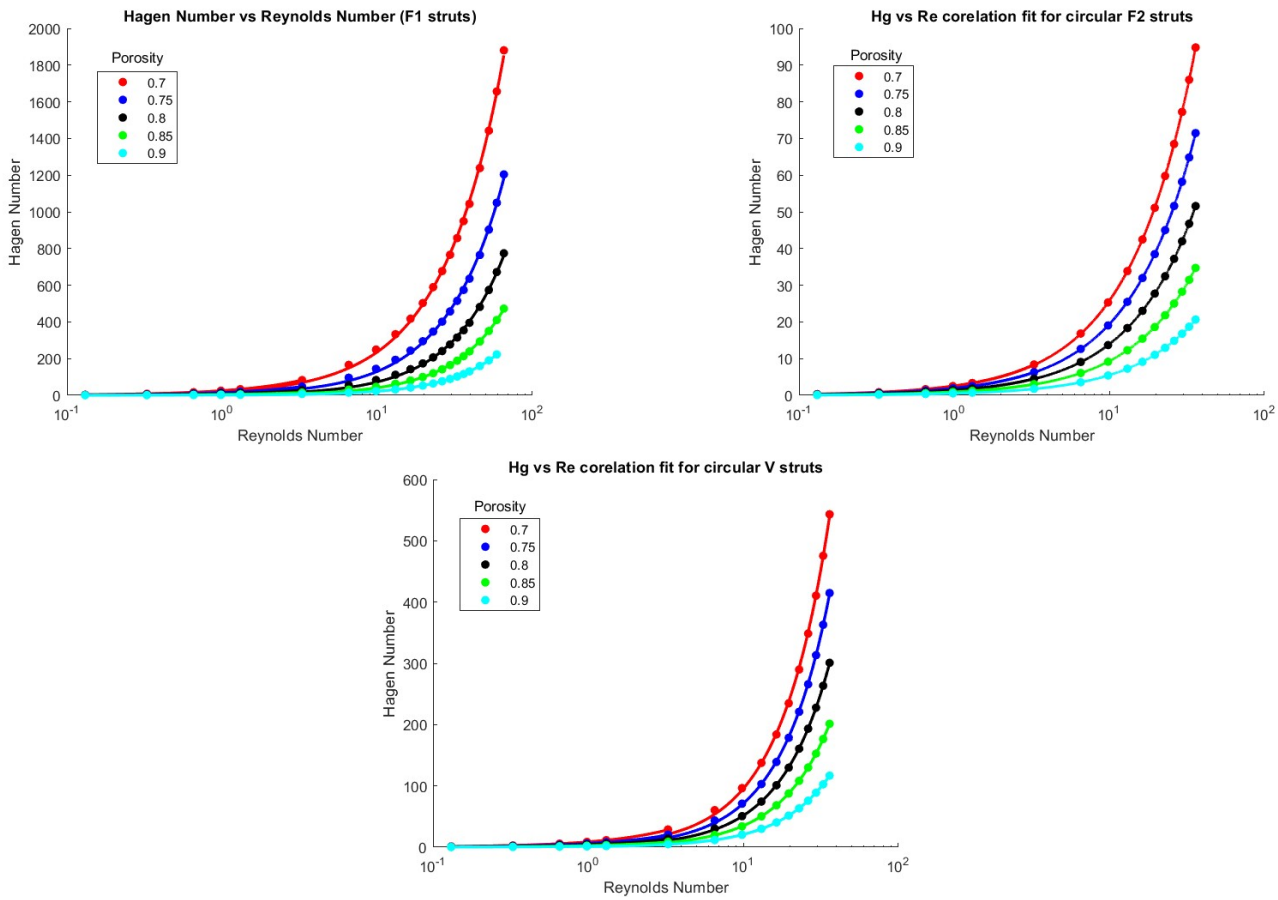

Figure 16: Curve fitting for Hg v Re correlations for circular struts

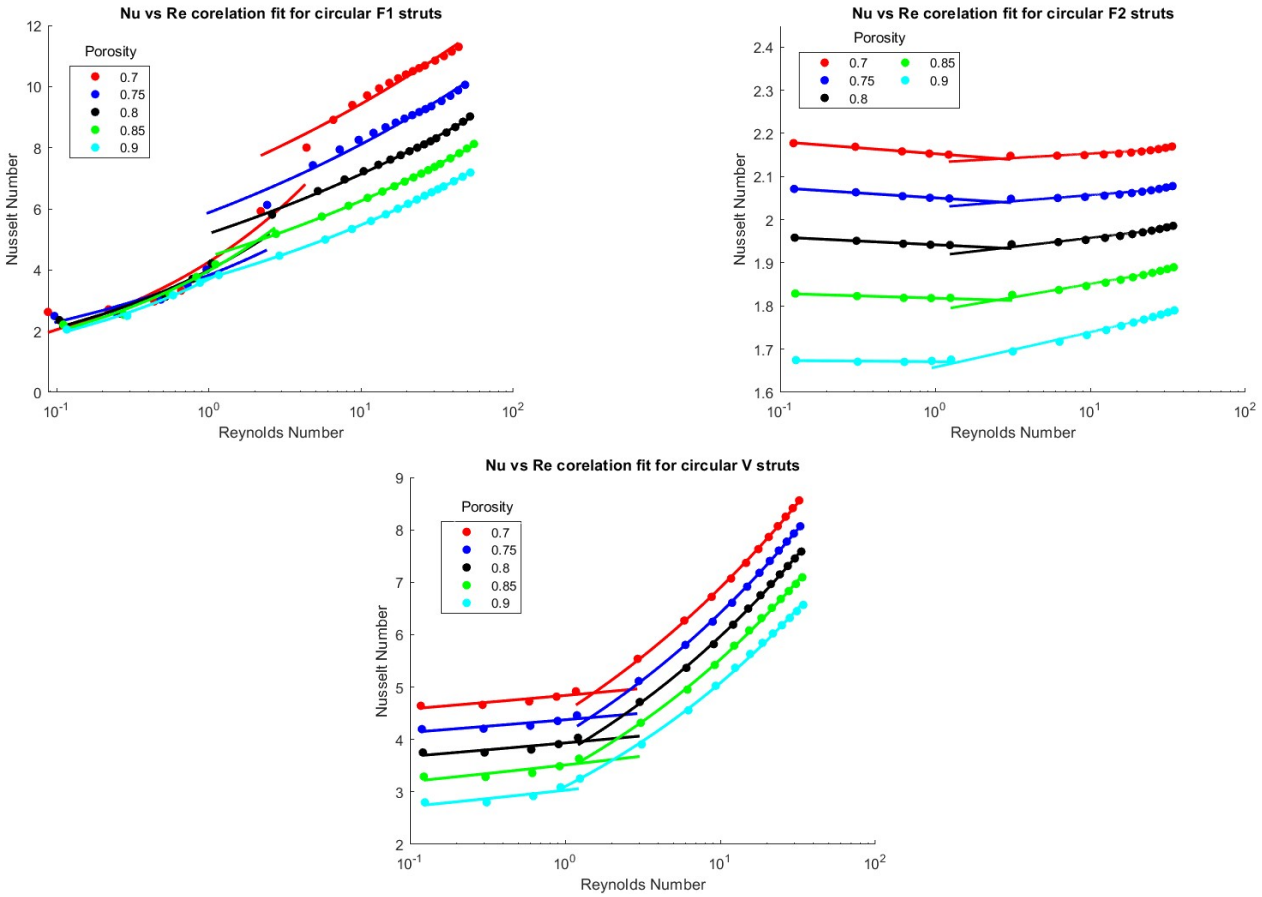

Figure 17: Curve fitting for Nu v Re correlations for circular struts

For the circular struts, it was observed that using the strut row porosity for given by equation 24 gives high errors while comparing the predictions using the superposition approach to the simulation results. Instead we use the concept of the inlet porosity instead of ψ_r. The inlet porosity is the available area for flow when viewed from the flow direction. With this definition, for all strut shapes we calculate the inlet porosity as $\psi_{in} = 1 - \frac{1}{sT}$. The difference between these two porosities is highlighted in Fig 15. The inlet porosity is used in case of the strut Hg as it is more relevant to the pressure drop while the strut row porosity is used for Nu as is related to the surface area which directly affects the heat transfer.

The calculated coefficients from this procedure are tabulated below

Strut Type	**Porosity**	**Nusselt Number**				**Hagen Number**			
		Regime 1		**Regime 2**		**Regime 1**		**Regime 2**	
		A	n	A	n	B	m	B	m
F1 Struts	0.7	3.37930	0.15641	5.89520	0.16323	25.28800	1.00000	18.93500	1.09630
	0.75	3.57850	0.22259	5.63240	0.13989	14.58200	1.00010	8.71190	1.17460
	0.8	3.74910	0.27864	5.03080	0.13810	8.32450	1.00020	4.10370	1.24980
	0.85	3.77660	0.30257	4.32990	0.14914	4.51390	1.00050	2.08530	1.29520
	0.9	3.57770	0.28827	3.66710	0.16551	2.16750	1.00080	1.09560	1.30270
F2 Struts	0.7	2.15360	-0.00557	2.13200	0.00414	2.55960	1.00020	2.47950	1.01670
	0.75	2.05110	-0.00487	2.02760	0.00607	1.92180	1.00030	1.85690	1.01850
	0.8	1.94220	-0.00396	1.91520	0.00935	1.37770	1.00040	1.32570	1.02150
	0.85	1.81830	-0.00257	1.78810	0.01479	0.91748	1.00060	0.87816	1.02600
	0.9	1.67100	-0.00068	1.65700	0.02077	0.53535	1.00070	0.50953	1.03300
V Struts	0.7	4.82760	0.02379	4.43310	0.18321	8.67700	1.00220	4.24560	1.35220
	0.75	4.36600	0.02472	4.03780	0.19329	6.07620	1.00350	3.04180	1.37060
	0.8	3.92500	0.02932	3.68910	0.20198	4.05540	1.00560	2.17330	1.37530
	0.85	3.50400	0.04097	3.37110	0.20904	2.51000	1.00950	1.50210	1.36660
	0.9	3.02480	0.04694	3.06990	0.21413	1.35190	1.01010	0.93565	1.34670

Table 8: Correlation coefficients for circular struts

Strut Shape	Porosity	Nusselt Number				Hagen Number			
		Regime 1		Regime 2		Regime 1		Regime 2	
		A	n	A	n	B	m	B	m
F1 Struts	0.65	3.5229	0.19113	5.8287	0.21129	53.188	1.0001	46.713	1.0451
	0.7	3.64300	0.25001	5.99890	0.16665	33.84600	1.00010	26.92000	1.08130
	0.75	3.74530	0.30102	5.65400	0.14550	20.25600	1.00030	14.48600	1.12140
	0.8	3.70740	0.30011	4.69530	0.15986	11.37900	1.00030	7.23120	1.16860
	0.85	3.58870	0.28939	4.14440	0.15917	6.13740	1.00020	3.49040	1.21970
	0.9	3.48110	0.30154	3.62780	0.16107	2.82490	1.00050	1.54230	1.25800
F2 Struts	0.65	2.28100	-0.00595	2.24670	0.00649	4.34380	1.00000	4.29730	1.00490
	0.7	2.18140	-0.00542	2.14530	0.00809	3.38810	1.00010	3.34270	1.00620
	0.75	2.07780	-0.00473	2.04030	0.00975	2.55320	1.00010	2.50710	1.00870
	0.8	1.96450	-0.00373	1.92580	0.01211	1.82960	1.00020	1.78580	1.01200
	0.85	1.83830	-0.00245	1.79940	0.01647	1.20940	1.00020	1.16660	1.01690
	0.9	1.68170	-0.00045	1.65880	0.02093	0.67905	1.00040	0.63630	1.02290
V Struts	0.65	5.02320	0.03073	4.64470	0.15301	11.64100	1.00110	8.42320	1.23730
	0.7	4.60170	0.03300	4.31210	0.16780	8.34090	1.00210	5.84910	1.28140
	0.75	4.19360	0.03597	3.98420	0.18019	5.87280	1.00270	4.11430	1.30590
	0.8	3.78960	0.03989	3.66540	0.19078	3.91360	1.00350	2.84630	1.31570
	0.85	3.40080	0.04489	3.36300	0.19931	2.48390	1.00510	1.97130	1.31410
	0.9	2.93950	0.04577	3.07530	0.20711	1.34290	1.00570	1.24740	1.30380

Table 9: Correlation coefficients for square struts

Strut Shape	Porosity	Nusselt Number				Hagen Number			
		Regime 1		Regime 2		Regime 1		Regime 2	
		A	n	A	n	B	m	B	m
F1 Struts	0.65	3.6085	0.23633	5.9704	0.20217	48.585	1.0001	41.711	1.0439
	0.7	3.69560	0.27365	6.18820	0.15845	30.64600	1.00010	23.72300	1.08120
	0.75	3.77880	0.31311	5.90800	0.13530	18.35700	1.00020	12.69700	1.12180
	0.8	3.71530	0.31240	4.97750	0.14553	10.15200	1.00030	6.00350	1.16940
	0.85	3.55270	0.29433	4.35280	0.14860	5.48630	1.00020	2.89090	1.22310
	0.9	3.38660	0.28400	3.74870	0.15737	2.49750	1.00030	1.25740	1.26990
F2 Struts	0.65	2.30420	-0.00491	2.27880	0.00715	4.14490	1.00000	4.08190	1.00530
	0.7	2.19520	-0.00420	2.16690	0.00844	3.20160	1.00010	3.13880	1.00670
	0.75	2.08530	-0.00342	2.05600	0.00995	2.40810	1.00010	2.34530	1.00910
	0.8	1.96340	-0.00239	1.93370	0.01198	1.72940	1.00020	1.66750	1.01260
	0.85	1.83680	-0.00098	1.80490	0.01645	1.14210	1.00020	1.08140	1.01710
	0.9	1.67860	0.00039	1.65170	0.02097	0.64221	1.00030	0.58156	1.02320
V Struts	0.65	5.13790	0.02527	4.67120	0.14543	11.51800	1.00130	8.14220	1.23480
	0.7	4.67350	0.02731	4.34130	0.15895	8.08260	1.00220	5.65570	1.28040
	0.75	4.22110	0.03029	4.01800	0.17091	5.68490	1.00280	3.94510	1.30560
	0.8	3.77460	0.03421	3.69930	0.18105	3.81560	1.00360	2.74480	1.31540
	0.85	3.33800	0.03894	3.38820	0.18985	2.43890	1.00500	1.89530	1.31400
	0.9	2.83390	0.04331	3.08140	0.19846	1.31090	1.00590	1.19710	1.30350

Table 10: Correlation coefficients for rotated square struts

6.3 Results

Applying the superpositon approach using the above calculated data, we obtain results as tabulated below. We calculate the mean absolute percentage error (MAPE) for the predicted Hagen and Nusselt numbers. An acceptable MAPE value for the Nusselt number is considered as 20% while it is taken to be 40% for the Hagen number.

Strut Shape	MAPE Hg	APE < 40 %	MAPE Nu	APE < 20 %
Circular	54.841	34.615 %	8.2939	85.333 %
Square	40.53	54.167 %	8.1762	86.456 %
Rotated Square	61.446	25 %	21.281	47.5 %

Table 11: Results of the superposition approach

The Hagen number in all cases is over predicted. This may be because of the use of the inlet Reynolds number to calculate Hg_i as defined in equation 21. Based on the superposition calculations it has been observed that the inlet Reynolds number is always higher than the normal Reynolds number. Replacing Re_{in} by Re the predictions for the Hagen number improve and are below 40%, tabulated below

Strut Shape	**MAPE Hg**	**APE < 40 %**
Circular	37.688	53.333 %
Square	32.531	63.542 %
Rotated Square	29.66	66.25 %

Table 12: Results for Hagen number predictions using Re

The comparison of the simulation data and the properties calculated from the superposition approach are represented in figures 18 and 20 for the Hagen number and the Nusselt number respectively.

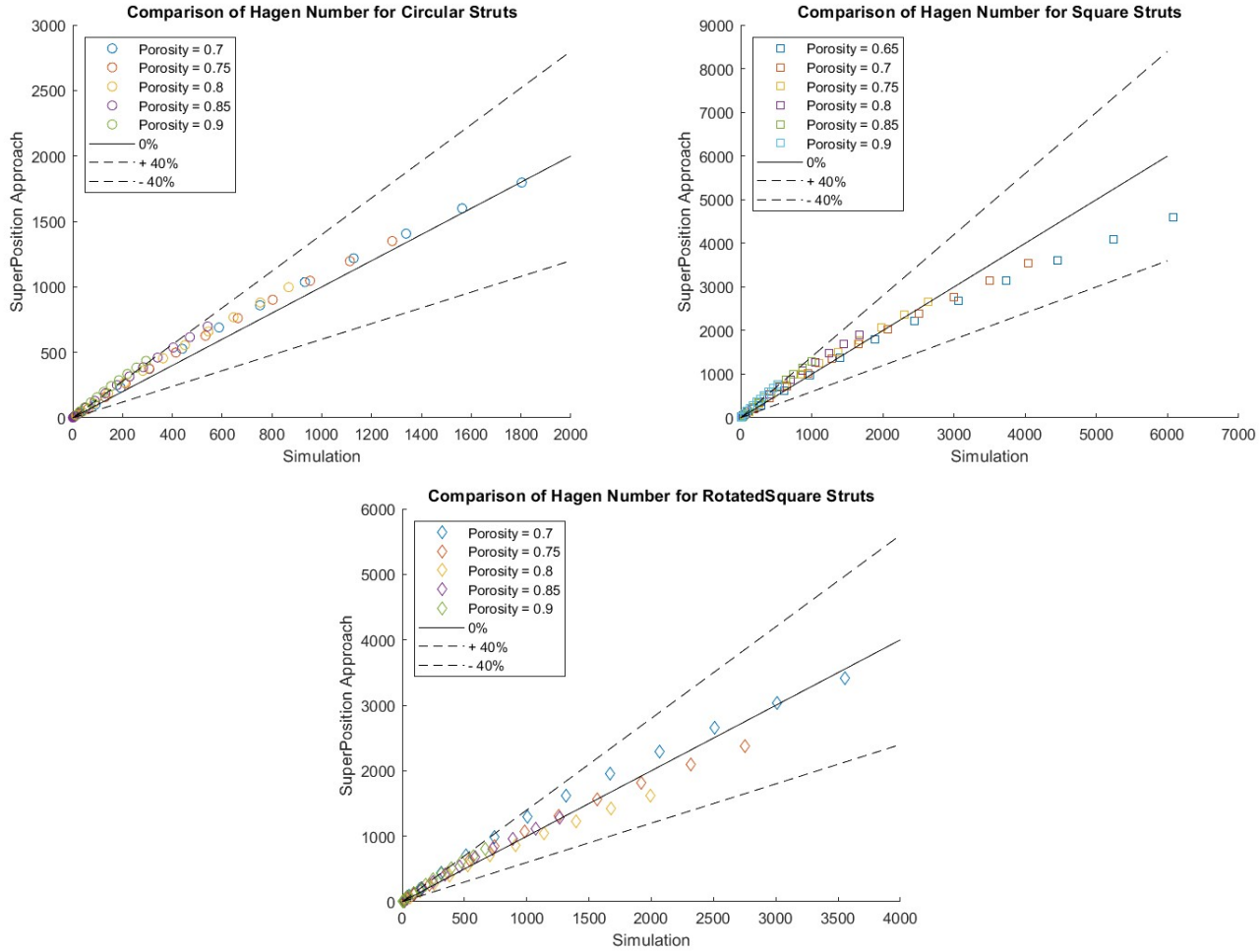

Figure 18: Comparison of results for the Hagen Number

From the results for the Hagen number, we can see that the predictions improve the most for the rotated square struts shape when Re_{in} is not used. This could be because the inlet porosity for the kelvin cell with the rotated square struts is the lowest and hence it has a larger influence on the inlet Reynolds number as indicated in Fig 19. Along with this, for all strut shapes at any given porosity the error in the predictions is highest in Regime 1 and is comparatively lower for Regime 2. The MAPE of the predictions in Regime 1 and Regime 2 are obtained as 59.37% and 29.16% for circular struts, 48.55% and 26.26% for square struts and 60.05% and 18.13% for rotated square struts. The error in the Hagen number is observed to increase with the porosity except for the rotated square struts where it first decreases and then increases. Considering the circular strut shape, the errors in Hg increase as 20.72%, 25.24%, 34.48%, 48.98%, 62.05% from porosity 0.7 to 0.9

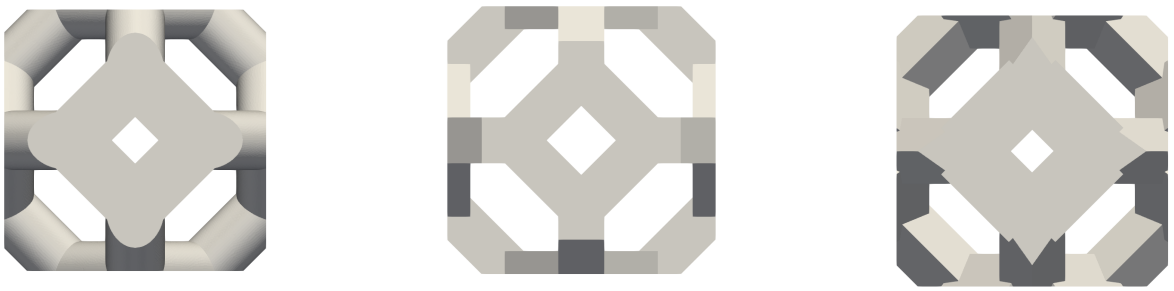

(a) $\psi_{in} = 0.725$ (b) $\psi_{in} = 0.758$ (c) $\psi_{in} = 0.658$

Figure 19: Inlet porosities of Kelvin cells with $\psi = 0.8$

For the Nusselt number, the predictions for the circular and the square strut shapes show an average error less than 10% but for the rotated square struts the error is higher. From the plots below, it can bee seen that the error increases at higher Reynolds numbers. This increase in error is observed for Regime 3 as explained in Fig 9d. The superposition approach under predicts the Nu values in Regime 3. As Regime 3 occurs at a lower Reynolds number for the rotated square struts, the prediction errors are larger. For the rotated square struts the errors are larger in Regime 1 as well. This can be explained by the regime boundary values given in equation 23. As these values are average values considering different unit cells without considering the possible effect of strut shapes on these regime boundaries, they may not be appropriate for the case of rotated square struts.

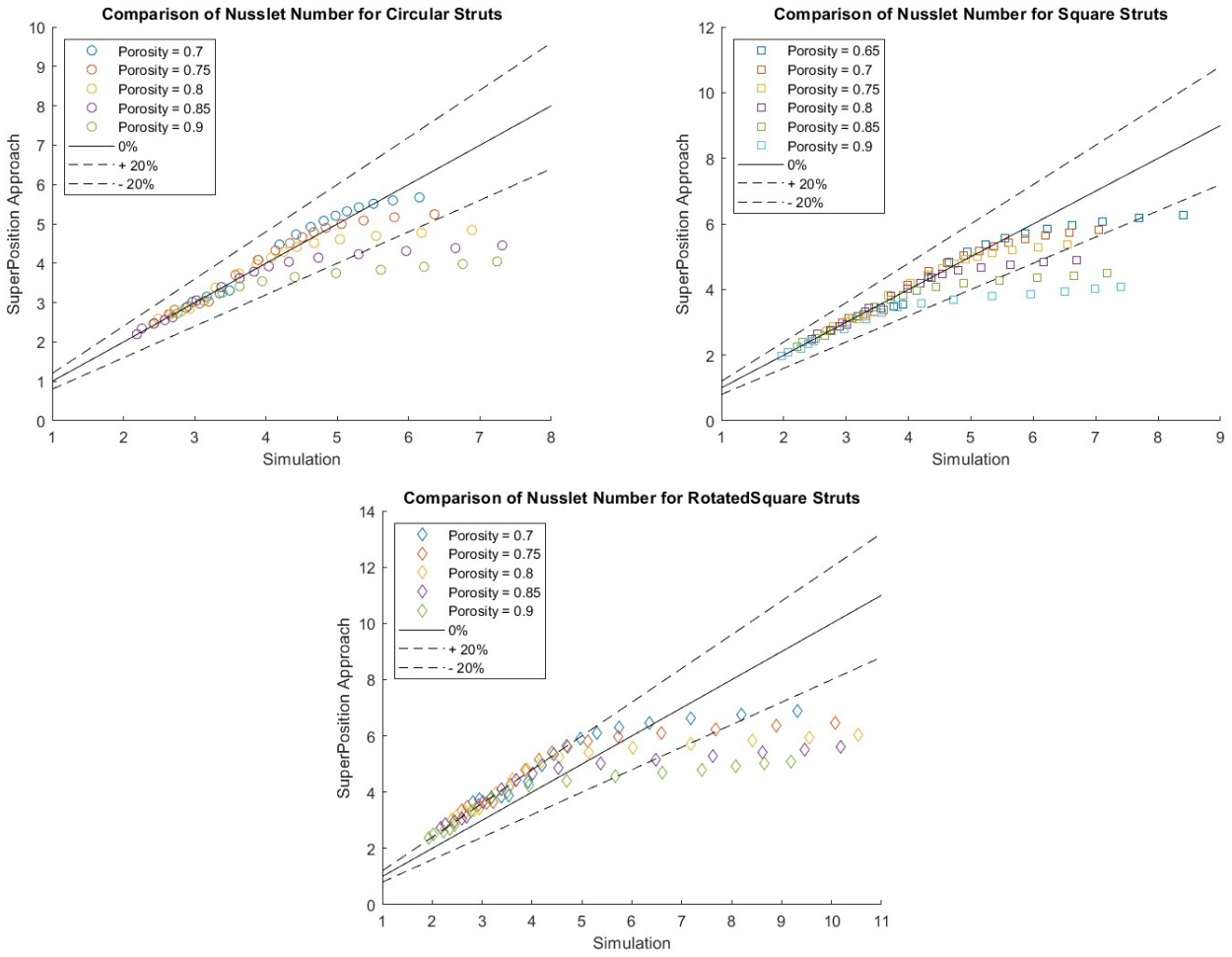

Figure 20: Comparison of results for the Nusselt Number

6.4 Remarks

The superposition approach develop by [3] is a general approach which was tested on various types of unit cells, showing good predictions. In this study, we consider the specific case of the Kelvin cell and considering the effect of different strut shapes which was not investigated for the superposition approach before. As this is a general approach, some improvements can be made specifically for the Kelvin cell to improve the applicability of the approach. Along with this some adaptations specific to the strut shape may be necessary. Some of the changes which have already been made to the approach include the usage of the inlet porosity for strut arrangements instead of the porosity given by equation 24. Along with this the inlet Reynolds number used in equation 21 has been replaced by the standard Reynolds number. Adapting these changes already improves the results of the superposition approach but there are a few more modifications that could be implemented.

As discussed previously, the predictions of the Nusselt number are poor in Regime 3, showing under predictions. The change in slope from Regime 2 to 3 is significant and cannot be completely described by the approach used. This can be explained based on the node factor in equation 26. This factor accounts for the reduction in available surface area as well as the stagnation zones induced by the nodes. But in Regime 3, at higher velocities this stagnation effect reduces, increasing the node factor. This node factor becomes Re dependent in Regime 3 and a new expression considering this dependency can be derived by curve fitting. This has been done in [3] again taking an average value of the node factor independent of the porosity for higher Re, but for Regime 4 which is the transient regime beyond the scope of this study. This significant change in slope for Regime 3 is a characteristic of the Kelvin cell and is not observed in all of the other unit cells such as the Cubic cell.

Another modification can come in the form of the regime boundaries. This further needs to be investigated considering a wider range of velocities and manually determining the regime boundaries at different porosities for different strut shapes. Considering the fit for the Nusselt number correlations in Fig 17 for the F1 struts, we can see that the points in Regime 1 do not exactly show constant Nu as expected in this regime. Simulations at further lower Reynolds number show that the constant Nu regime exists only at lower Re than calculated from the regime boundaries. With this it could be possible to derive strut shape dependent regime boundary definitions for the Kelvin cell. Although these adaptations to the approach are specific to the Kelvin cell and will increase the complexity of the superposition approach which was developed to accommodate all types of POCS, they would make the predictions more accurate. The changes proposed above will be tested and compared to the existing results in further studies.

7 Conclusions

In this work we have investigated the hydrodynamic and convective heat transfer properties of Kelvin cell based POCS, considering the effect of different strut shapes. It was shown that the pressure drop and heat transfer coefficient follow the same order, highest for the rotated square struts and lowest for the circular struts. Hence there is a trade off between the pressure drop and heat transfer and the choice of strut shape for a specific application must be made considering the maximum allowable pressure drop. We test various length scales to derive dimensionless plots for the Nusselt and Hagen number which can be used to develop correlations for these quantities.

Further, we discuss and apply the superposition approach which gives satisfactory results for all strut shapes for predictions of both, the Hagen number and the Nusselt number. Suggestions to tune this approach for the case of Kelvin cell and to accommodate different strut shapes have been presented and will be tested in further investigations

References

[1] G. Ambrosio, N. Bianco, W. K. Chiu, M. Iasiello, V. Naso, and M. Oliviero. The effect of open-cell metal foams strut shape on convection heat transfer and pressure drop. *Applied Thermal Engineering*, 103:333–343, 2016.

[2] E. Bianchi, W. Schwieger, and H. Freund. Assessment of periodic open cellular structures for enhanced heat conduction in catalytic fixed-bed reactors. *Advanced Engineering Materials*, 18:n/a–n/a, 09 2015.

[3] K. Dubil. *Modelling of heat transport in periodic open cell structures with single-phase, laminar flow.* PhD thesis, Karlsruher Institut für Technologie (KIT), 2023.

[4] K. Dubil, T. Wetzel, and B. Dietrich. Modelling steady-state convective heat transfer in different periodic open cellular structures (pocs) – a superposition approach. *International Journal of Heat and Mass Transfer*, 200:123546, 2023.

[5] C. Ferroni, M. Bracconi, M. Ambrosetti, M. Maestri, G. Groppi, and E. Tronconi. A fundamental investigation of gas/solid heat and mass transfer in structured catalysts based on periodic open cellular structures (pocs). *Industrial & Engineering Chemistry Research*, 60(29):10522–10538, 2021.

[6] C. Ferroni, F. S. Franchi, M. Ambrosetti, M. Bracconi, G. Groppi, M. Maestri, and E. Tronconi. Numerical and experimental investigation of pressure drop in periodic open cellular structures for intensification of catalytic processes. *ACS Engineering Au*, 2(2):118–133, 2022.

[7] M. Iasiello, S. Cunsolo, N. Bianco, W. Chiu, and V. Naso. Developing thermal flow in open-cell foams. *International Journal of Thermal Sciences*, 111:129–137, 2017.

[8] P. Kumar and F. Topin. Micro-structural impact of different strut shapes and porosity on hydraulic properties of kelvin-like metal foams. *Transport in Porous Media*, 105, 10 2014.

[9] P. Kumar and F. Topin. State-of-the-art of pressure drop in open-cell porous foams: Review of experiments and correlations. *Journal of Fluids Engineering*, 139:111401–13, 06 2017.